CRYSTAL GROWTH & DESIGN

Article

pubs.acs.org/crystal

Multiple Crystal Forms of *p*-Aminosalicylic Acid: Salts, Salt Co-Crystal Hydrate, Co-Crystals, and Co-Crystal Polymorphs

Published as part of the Crystal Growth & Design virtual special issue In Honor of Prof. G. R. Desiraju

Pramod Kumar Goswami,[†] Ram Thaimattam,*[,‡] and Arunachalam Ramanan*[,†]

[†]Department of Chemistry, Indian Institute of Technology Delhi, Hauz Khas, New Delhi-110016, India

[‡]Ranbaxy Laboratories Ltd., Chemical Research, Plot-20, Sector-18, Udyog Vihar Industrial Area, Gurgaon-122015 (Haryana), India

Supporting Information

ABSTRACT: Crystallization of *p*-aminosalicylic acid, an anti-tuberculosis drug, in the presence of pyridine derivatives as coformers led to formation of nine multicomponent solids that include salts, a salt co-crystal hydrate, co-crystals, and co-crystal polymorphs. Seven of them are new solid forms. The influence of the COOH···$N_{heterocycle}$ synthon is examined in dictating the various crystal forms, the manifestation of which depends on solvent of crystallization and API-coformer composition in solution.

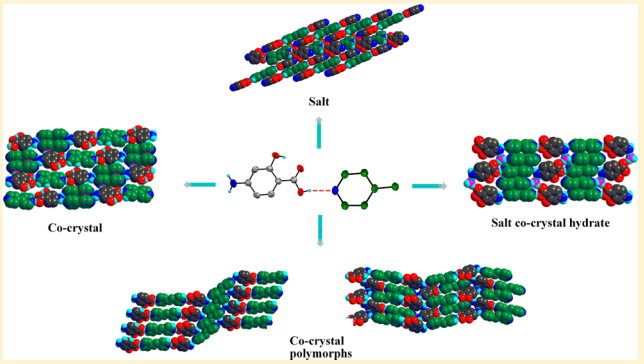

INTRODUCTION

Active pharmaceutical ingredient (API) co-crystals have demonstrated the ability to modify physicochemical properties of the APIs.[1] *p*-Aminosalicylic acid (PAS) is a well-known antibiotic in tuberculosis (TB) treatment and also a promising anticancer drug.[2] Recently, there is a renewed interest in obtaining the multicomponent crystals based on this molecule to explore its solid state chemistry.[3] PAS is also a potential ligand in the context of coordination polymers with multi-dentating functionality to stabilize metal ions in solution, and along with bridging ligands such as like 4,4′-bipyridine (*bpy*) or its analogues, it can lead to multidimensional extended structures.[4] PAS is one of the components of the anti-TB combination drug used in second-line therapy. Recently PAS is reported to form an unexpected salt co-crystal with *bpy* and interesting drug-drug co-crystals with other anti-TB drugs, isoniazid and pyrazinamide, used in first-line treatment to prevent multiple drug-resistant TB.[2,5,6a] The reported crystal structure of PAS with *bpy* is quite unusual in that both charged and neutral *bpy* species are present in the same crystal.[5a] There is a single hydrogen bond, COOH···$N_{heterocycle}$ synthon,[6b] between PAS and *bpy* that is distinct from the commonly found two-point hydrogen bonded COOH···$N_{heterocycle}$ interaction wherein the interacting moieties are in the same plane. The COOH···$N_{heterocycle}$ synthon is also found to be the driving force for the formation of PAS-isoniazid and PAS-pyrazinamide drug-drug co-crystals.[6a] A 2:1 PAS/*bpy* salt/co-crystal involving PAS···*bpy*···PAS trimer connected by COOH···$N_{heterocycle}$ is generally expected if they are co-crystallized. For instance, this is demonstrated in ibuprofen-*bpy* co-crystals.[7] This prompted us to further explore the structural landscape of the PAS-pyridine/*bpy* derivative system. Therefore, co-crystal formation of PAS with *bpy*, 4-amino pyridine (*pap*), 3-hydroxy pyridine (*mhp*), 1,2-bis(4-pyridyl)ethane (*bpe*), and 1,2-bis(4-pyridyl)-ethylene (*bpee*) were explored. In this paper, we describe 2:1 co-crystal of PAS and *bpy* (**1**), 2:3 co-crystal of PAS and *bpy* (**2**), 1:2 salt co-crystal monohydrate of PAS and *bpy* (**2a**), 1:1 salts of PAS and *pap* (**3**), and PAS and *mhp* (**4**), 2:1 salt of PAS and *bpe* (**5**), two polymorphs of 1:1 co-crystal of PAS and *bpe* (**6** and **6a**), and 1:1 co-crystal of PAS and *bpee* (**7**).

EXPERIMENTAL SECTION

All reagents and solvents were used as received from commercial suppliers without further purification. All nine of the solid forms were obtained by slow evaporation of acetone or acetone-MeOH mixtures. The solutions were prepared by dissolving the components in the solvent or solvent mixture, or by slowly adding a clear solution of the coformer to the API solution. Stoichiometry of the components in the solution had an effect on the outcome (Table 3).

Synthesis of PAS·(*bpy*)$_{0.5}$, 1. PAS (0.65 mmol, Merck 99%) was dissolved in 7 mL of acetone (Merck 99%) followed by the addition of 4 mL of solution of *bpy* (0.32 mmol, Merck 99%). The resulting yellow color solution was stirred and kept at room temperature for crystallization. Yellow plate shaped crystals of **1** after 4−5 days in about 85% yield (based on PAS) were filtered and dried in desiccators. Elem. Anal. (%) Calcd for **1**: C, 62.06; H, 5.21; N, 12.06. Found: C, 62.41; H, 4.73; N, 12.18. IR (cm^{-1}): 3460 (s), 3366 (s), 3233 (s),

Received: October 18, 2012
Revised: November 14, 2012

 © XXXX American Chemical Society dx.doi.org/10.1021/cg3015332 | *Cryst. Growth Des.* XXXX, XXX, XXX−XXX

1633 (s), 1576 (s), 1506 (m), 1413 (m), 1370 (m), 1330 (w), 1253 (s), 1146 (s), 1060 (s), 1003 (m), 966 (s), 830 (w), 780 (s).

Synthesis of PAS·(*bpy*)$_{1.5}$, 2. Solution of PAS (0.32 mmol) was prepared in 10 mL of acetone. To the above solution *bpy* (0.65 mmol) was added slowly. The resulting solution was stirred and kept at room temperature for crystallization. Plate shaped yellow crystals of **2** in about 80% yield (based on PAS) were obtained after 3 days. Elem. Anal. (%) Calcd for **2**: C, 68.03; H, 5.19; N, 14.12. Found: C, 67.89; H, 4.84; N, 14.35. IR (cm^{-1}): 3333 (s), 3213 (s), 1643 (s), 1583 (s), 1396 (s), 1333 (m), 1213 (s), 1156 (m), 1056 (s), 963 (m), 836 (s), 796 (s).

Synthesis of PAS·*pap*, 3. To a 5 mL solution of PAS (0.65 mmol) in acetone was added a solution of *pap* (0.65 mmol, Merck 99%) in 5 mL. Yellow plate shaped crystals of **3** in about 75% yield (based on PAS) collected after 5 days of slow evaporation under ambient conditions. Elem. Anal. (%) Calcd for **3**: C, 58.29; H, 5.30; N, 16.99. Found: C, 57.26; H, 5.37; N, 17.18. IR (cm^{-1}): 3433 (s), 3321 (s), 3219 (s), 1644 (s), 1525 (m), 1506 (m), 1435 (s), 1358 (m), 1196 (s), 1155 (m), 990 (m), 819 (s), 778 (m), 702 (m).

Synthesis of PAS·*mhp*, 4. Five milliliters of acetone solution of *mhp* (0.65 mmol, Merck 99%) was mixed to 7 mL acetone solution of PAS (0.65 mmol), and the light yellow clear colored solution was kept for slow evaporation at room temperature. Yellow colored plate shaped crystals in about 85% yield (based on PAS) were obtained after 5 days. Elem. Anal. (%) Calcd for **4**: C, 58.06; H, 4.87; N, 11.29. Found: C, 58.08; H, 4.84; N, 11.62. IR (cm^{-1}): 3413 (m), 3340(m), 3220 (m), 1630 (w), 1575 (s), 1503 (s), 1433 (m), 1361 (s), 1277 (s), 1157 (s), 1096 (w), 963 (w), 830 (m), 699 (m).

Synthesis of PAS·(*bpe*)$_{0.5}$, 5. A solution of PAS (0.65 mmol) was prepared in 10 mL of acetone. Five milliliters of acetone solution of *bpe* (0.32 mmol, Merck 99%) was added to the above solution. The resulting solution was stirred and kept at room temperature for crystallization. Needle shaped yellow crystals of **5** in about 80% yield (based on PAS) were obtained after 7 days. Elem. Anal. (%) Calcd for **5**: C, 63.66; H, 5.34; N, 11.42. Found: C, 64.16; H, 5.27; N, 11.99. IR (cm^{-1}): 3400 (s), 3340 (s), 3240 (s), 1630 (s), 1581 (s), 1305 (m), 1276 (s), 1150 (s), 1090 (w), 782 (m).

Synthesis of PAS·*bpe*, 6. PAS (0.65 mmol) was dissolved in 7 mL of acetone and to this solution 5 mL acetone solution of *bpe* (0.97 mmol) was mixed slowly. The solution was kept at room temperature for crystallization. Plate shaped crystals of **6** in about 70% yield (based on PAS) were obtained after 5 days. Elem. Anal. (%) Calcd for **6**: C, 67.64; H, 5.68; N, 12.46. Found: C, 68.20; H, 5.79; N, 13.09. IR (cm^{-1}): 3460 (s), 3313 (s), 3166 (s), 2980 (m), 1633 (m), 1597 (s), 1503 (s), 1414 (s), 1335 (m), 1193 (s), 1151 (m), 1033 (s), 993 (w), 820 (s).

Synthesis of PAS·*bpe*, 6a. Seven milliliter acetone solution of PAS (0.65 mmol) was mixed slowly with 4 mL acetone solution of *bpe* (0.65 mmol). Plate shaped crystals of **6a** in about 90% yield (based on PAS) were obtained at room temperature after 3 days. Elem. Anal. (%) Calcd for **6a**: C, 67.64; H, 5.68; N, 12.46. Found: C, 68.32; H, 5.81; N, 13.16. IR (cm^{-1}): 3465 (s), 3387 (s), 3304 (s), 3194 (s), 2928 (m), 1640 (s), 1511 (s), 1420 (m), 1387 (m), 1294 (s), 1228 (m), 1195 (m), 1157 (m), 1040 (s), 829 (s).

Synthesis of PAS·*bpee*, 7. PAS (0.65 mmol) was dissolved in 10 mL of acetone and to this solution 4 mL acetone solution of *bpee* (0.65 mmol) was mixed slowly .The solution was stirred and kept at room temperature for crystallization. Plate shaped crystals of **7** were obtained after 2 days. IR (cm^{-1}): 3426 (m), 3306 (m), 3146 (m), 3033 (m), 2973 (m), 1633 (m), 1595 (s), 1415 (s), 1250 (s), 1195 (w), 1140 (m), 997 (m), 824 (s).

X-ray Structure Determination. X-ray diffraction studies of crystal mounted on a capillary were carried out on a BRUKER AXS SMART-APEX diffractometer with a CCD area detector (Kα = 0.71073 Å, monochromator: graphite).[8] Frames were collected at T = 150 K by ω, ϕ and 2θ-rotation at 10 s per frame with SAINT.[9] The measured intensities were reduced to F^2 and corrected for absorption with SADABS.[9] Structure solution, refinement, and data output were carried out with the SHELXTL program.[10] Non-hydrogen atoms were refined anisotropically. C−H hydrogen atoms were placed in geometrically calculated positions and refined as riding atoms. O−H and N−H hydrogen atoms were located from difference Fourier maps and refined isotropically. Images were created with the Diamond program.[11] Hydrogen bonding interactions in the crystal lattice were calculated with SHELXTL. Crystal and refinement data are summarized in Tables 1 and 2.

Table 1. Crystal Data and Structural Refinements for 1, 2, and 3

parameter	1	2	3
formula	PAS·(*bpy*)$_{0.5}$	PAS·(*bpy*)$_{1.5}$	PAS·*pap*
formula wt, g mol^{-1}	462.46	774.82	247.25
T (K)	150(2)	150(2)	150(2)
wavelength (Å)	0.71073	0.71073	0.71073
crystal system	monoclinic	triclinic	orthorhombic
space group	$P2_1/c$	$P\bar{1}$	$Pbca$
a (Å)	5.418(3)	8.191(3)	13.397(4)
b (Å)	8.764(5)	10.755(3)	12.547(4)
c (Å)	23.315(13)	11.897(4)	13.879(4)
α (°)	90.00	74.000(6)	90.00
β (°)	91.321(11)	84.991(6)	90.00
γ (°)	90.00	76.519(6)	90.00
V (Å^3)	1106.7(1)	979.5(5)	2333.2(6)
Z	2	1	8
d_{calc} (g cm^{-3})	1.388	1.314	1.408
μMoKα (cm^{-1})	0.102	0.090	0.104
R_{int}	0.0494	0.0352	0.0522
R_1 ($I > 2\sigma I$)	0.0967	0.1021	0.0638
wR_2 (all)	0.1971	0.2043	0.1281
GOF	1.248	1.232	1.256
CCDC no.	905631	905632	905634

Table 2. Crystal Data and Structural Refinements for 4, 5, 6, and 7

parameter	4	5	6	7
formula	PAS·*mhp*	PAS·(*bpe*)$_{0.5}$	PAS·*bpe*	PAS·*bpee*
formula weight, g mol^{-1}	248.24	490.51	337.37	335.36
T (K)	150(2)	150(2)	150(2)	150(2)
wavelength (Å)	0.71073	0.71073	0.71073	0.71073
crystal system	orthorhombic	monoclinic	monoclinic	triclinic
space group	$Pca2_1$	$P2_1/n$	$P2_1/n$	$P\bar{1}$
a (Å)	12.951(4)	7.949(3)	11.196(3)	6.2977
b (Å)	5.1138(15)	11.747(4)	8.041(2)	9.1148
c (Å)	17.068(5)	12.875(3)	19.179(6)	15.243
α (°)	90.00	90.00	90.00	72.801
β (°)	90.00	103.417(6)	96.644(6)	84.100
γ (°)	90.00	90.00	90.00	77.889
V (Å^3)	1130.5(6)	1169.3(7)	1715.0(9)	816.5
Z	4	2	4	2
d_{calc} (g cm^{-3})	1.459	1.395	1.307	1.364
μMoKα (cm^{-1})	0.111	0.101	0.090	0.094
R_{int}	0.0418	0.0502	0.0867	0.0202
R_1 ($I > 2\sigma I$)	0.0720	0.0572	0.0848	0.0363
wR_2 (all)	0.1507	0.1567	0.1865	0.0976
GOF	1.291	1.043	1.098	1.047
CCDC no.	905635	905636	905637	905639

dx.doi.org/10.1021/cg3015332 | Cryst. Growth Des. XXXX, XXX, XXX−XXX

Other Physical Measurements. ATR-FTIR was recorded on a Perkin-Elmer spectrum one spectrometer (Figure S1, Supporting Information). Elemental analyses (C, H, N) were determined on Perkin-Elmer 2400 series II C, H, N analyzer. DSC analysis was carried out using Perkin−Elmer DSC system on well ground samples in flowing nitrogen atmosphere with a heating rate of 5 °C/min. All the solid forms of PAS show a single endothermic peak in DSC (Table 3 and Figure S2, Supporting Information). Room-temperature powder X-ray diffraction data were collected on a Bruker D8 Advance diffractometer using Ni-filtered CuKα radiation. Data were collected with a step size of 0.05° and at count time of 1 s per step over the range $2° < 2\theta < 60°$. Rietveld powder diffraction analysis of all the powders were carried out using TOPAS 4.2, Bruker for ensuring homogeneity of the synthesized products.[12]

Table 3. Composition and Physical Properties of Salts/Co-Crystals Based on PAS

composition in solution (PAS:coformer)	composition in solid	color and morphology	m.p. (°C) (from DSC)
2:1	PAS·$(bpy)_{0.5}$ **1**	yellow, plate	157
1:2	PAS·$(bpy)_{1.5}$ **2**	yellow, plate	162
1:1	PAS·*pap* **3**	yellow, plate	167
1:1	PAS·*mhp* **4**	yellow, plate	122
2:1	PAS·$(bpe)_{0.5}$ **5**	yellow, needle	142
2:3	PAS·*bpe* **6**	yellow, plate	145
1:1	PAS·*bpe* **6a**	yellow, plate	140

RESULTS AND DISCUSSION

In this study, we explored the utility of the well-known COOH···$N_{heterocycle}$ synthon in crystallizing multiple forms of the drug molecule, PAS with pyridine and *bpy* based coformers. Crystallization was carried out at ambient conditions but with different mole ratios of API to coformer in selected solvents. We isolated several new solids (Scheme 1) based on PAS. When PAS was reacted with *bpy* in acetone, we obtained two new co-crystals **1** (2:1 PAS:*bpy*) and **2** (2:3 PAS:*bpy*), and a known salt co-crystal hydrate, **2a** (1:2:1 PAS:*bpy*:water)[5b] depending on the mole ratio of PAS/*bpy* and solvent of crystallization. Crystal structures of both **1** and **2** showed the domination of COOH···$N_{heterocycle}$ synthon in dictating the supramolecular aggregation (Figure 1). Location of the acidic proton via Fourier map and further refinements is consistent with the two C−O bond lengths of the neutral group in **1** and **2**. In addition, in both cases, PAS···*bpy*···PAS trimer formed between *bpy* and a pair of PAS molecules is responsible for the formation of co-crystals (Figures 1 and 2). On closer inspection, it became evident that the relative orientations of the three interacting molecules in the trimer are different in **1** and **2**, which are connected by COOH···$N_{heterocycle}$ synthons I and II respectively (Scheme 2). In other words, the aromatic ring planes of interacting species are out of plane[13] in **1** while they are in plane[14] in **2**. Retrosynthesis of **1** and **2** showed how the system judiciously engineers the compositional variation through N−H···O interactions by adopting different kinds of growth for the trimer observed in the two solids (Table 4). In **1**, the trimers are interconnected by N−H···O, C−H···π hydrogen bonds generating ribbons, which in turn are interconnected via N−H···N hydrogen bonds generating layers parallel to $(\bar{1}04)$ planes that stack to generate the crystal structure stabilized by C−H···O and C−H···π interactions (Figure 1). In **2**, the additional two *bpy* molecules bridge the trimers through synthon III to generate linear chains (Figure 2). The two *bpy* molecules in synthon III also interact with each other via $\pi\cdots\pi$ interactions. The occurrence of *bpy* molecules in this configuration is quite rare. A Cambridge Structural Database (CSD) analysis revealed that synthon III does not occur in any of the *bpy* based solids. The linear chains in **2** are interconnected by C−H···O, C−H···N, and C−H···π interactions generating layers parallel to $(11\bar{2})$ planes which stack to complete the structure stabilized by C−H···O and C−H···π interactions.

Reacting PAS with another coformer, *pap* yielded a 1:1 salt, **3**. Here, as expected, $PAS^{-}-papH^{+}$ dimer is formed. In the dimer the ions are connected by synthon IV (Figure 3). The donor rich $PAS^{-}-papH^{+}$dimers close pack in the crystal connected by N−H···π and several N−H···O and hydrogen bonds. Reaction of PAS with *mhp* led to a 1:1 $PAS^{-}/mhpH^{+}$ salt, **4**. Crystal structure of **4** also showed the occurrence of a synthon IV based dimer. These dimers aggregate to form linear chains connected by O−H···O hydrogen bonds involving the pyridine OH group (Figure 4). The dimers are perpendicularly oriented in the chain, and the chains closely pack to generate bilayers parallel to the *ab* plane. The chains within the bilayer are connected by N−H···O hydrogen bonds involving the amino group. The bilayers are stacked along [001] connected by N−H···O and C−H···O hydrogen bonds. We could not identify any other forms for PAS−*pap* and PAS−*mhp* systems by varying composition and solvent.

We examined another coformer, *bpe*, which is a modification of *bpy* with a larger spacing. Like *bpy*, the reaction resulted in the crystallization of two solids with varying composition: a 2:1 salt **5** and a 1:1 co-crystal **6**. The trimer in **5** was similar to the one observed in **2** but with the proton located on the pyridine N-atom. Thus the molecules are connected by synthon IV in the trimer. However, these trimers do not self-assemble to form any discernible H-bonded network structure. The discrete trimers are stacked in an inclined manner along [001] as shown in (Figure 5). Alternating stacks of these trimers, related by about 90° rotation about [001], generate a bilayer parallel to $(\bar{2}20)$. These bilayers stack in such a way that the linear stacks of timers are close packed in a herringbone fashion. The inter- and intra-bilayer interactions are stabilized by N−H···O and C−H···π hydrogen bonds. The crystal structure of **6**, that is, 1:1

Scheme 1. Crystallization of Multiple Forms of the API, *p*-Aminosalicylic Acid (PAS) with Different Coformers under Varying API-Coformer Composition and Solvent of Crystallization

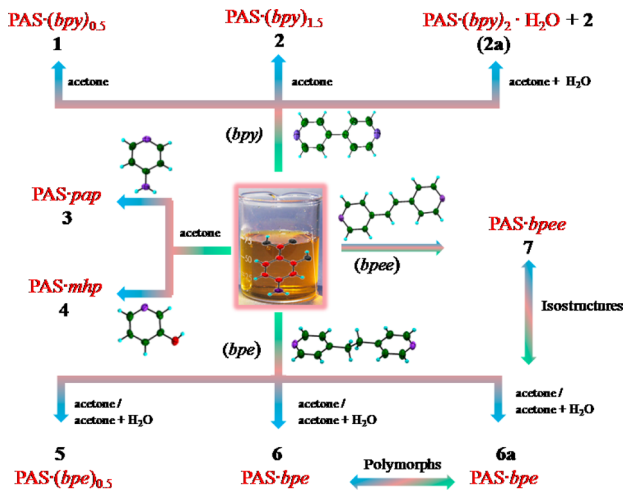

dx.doi.org/10.1021/cg3015332 | Cryst. Growth Des. XXXX, XXX, XXX−XXX

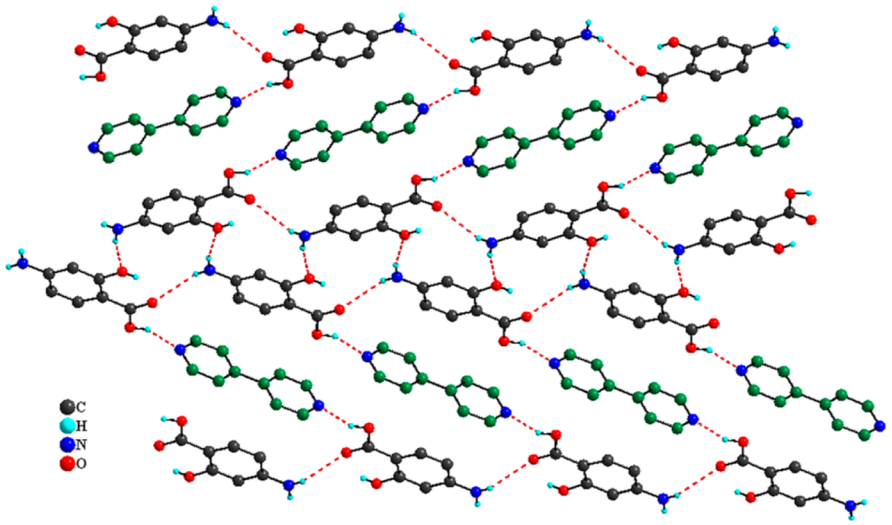

Figure 1. 2:1 Co-crystal of PAS and *bpy* (**1**). PAS···*bpy*···PAS trimers made of COOH···$N_{heterocycle}$ synthon I occur as ribbons. The aromatic ring planes of the interacting molecules in the trimers are out of plane. The trimers from each ribbon are oriented at angles and interact with each other through N−H···O involving the hydroxyl group PAS. In this and in the subsequent figures, the C-atoms of coformers are rendered green. H-bonds are shown in dashed lines and the H-atoms that are not involved in hydrogen bonding are omitted for clarity.

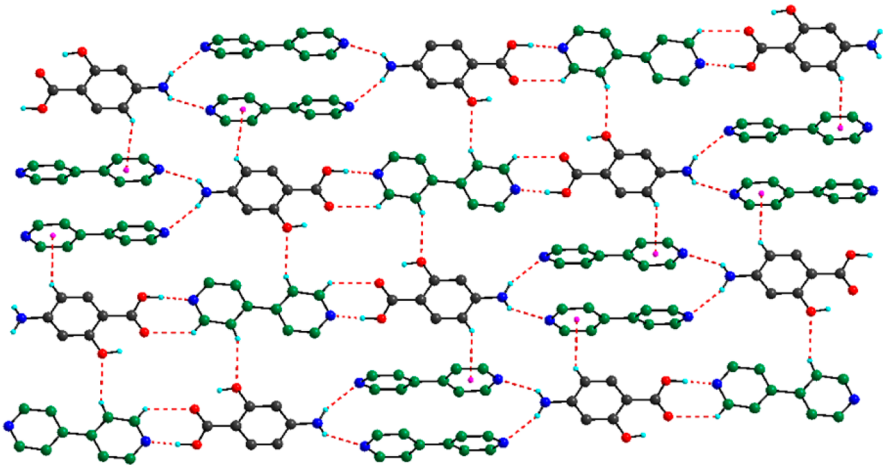

Figure 2. 2:3 Co-crystal of PAS and *bpy* (**2**). The PAS···*bpy*···PAS trimers are formed through COOH···$N_{heterocycle}$ synthon II. Unlike **1**, the aromatic ring planes of the interacting molecules are in plane. The two additional *bpy* molecules in **2** in comparison to **1** are bridging the trimers through synthon III forming infinite chains. C−H···O and C−H···π interactions link the chains into layers providing further stability to the solid.

Scheme 2. Synthons Observed in Various Crystal Forms Isolated in This Study

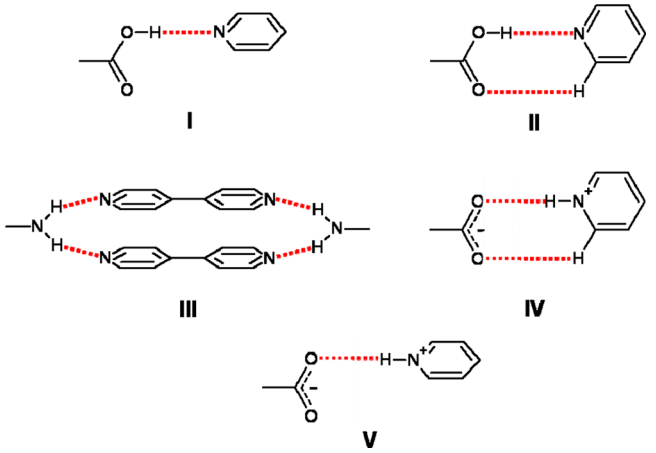

co-crystal with *bpe*, showed a different arrangement in comparison to **2**. The flexibility of C_{sp3}−C_{sp3} in *bpe* does not allow the packing as in **2** by accommodating additional *bpy* molecules in the crystal. Instead, the acid and pyridine derivatives alternatively interact forming 1-D chains. The PAS−*bpe* dimers, connected by synthon II, aggregate linearly linked by N−H···N hydrogen bonds (Figure 6). These chains are interconnected by N−H···π and C−H···π interactions generating planes parallel to (103) that are stacked to generate the crystal structure stabilized by C−H···O hydrogen bonds. Surprisingly, in contrast to *bpy*, the reaction with *bpe* with a different acid/base ratio yielded a polymorph of the 1:1 co-crystal, **6a** (Table 3). A close examination of the crystal structure suggested that it is the same solid reported earlier.[5b] Like in **6**, the acid and base molecules in **6a** are arranged alternatively in a chain (Figure S10). An essential difference is in the orientation of one of the PAS molecules in each chain and the interaction between the adjacent chains. In **6a**, unlike **6**, the PAS···*bpe*···PAS trimers, connected by synthon II, dominate

dx.doi.org/10.1021/cg3015332 | *Cryst. Growth Des.* XXXX, XXX, XXX−XXX

Table 4. Selected Hydrogen Bond Geometries for Normalized H-Atom Positions

	interaction	H···A (Å)	D···A (Å)	D−H···A (deg)
PAS·$(bpy)_{0.5}$	O1−H1···N2	1.828	2.654	155.2
	N1−H3···O2	2.480	3.206	148.5
	N1−H4···O3	2.329	3.093	165.2
	C4−H5···π	3.793	4.376	123.4
PAS·$(bpy)_{1.5}$	O1−H1···N4	1.658	2.626	174.8
	N1−H3···N2	2.328	3.034	142.3
	N1−H4···N3	2.269	3.108	156.6
	O3−H11···C21	2.516	3.326	145.7
	C4−H6···π	2.966	3.786	147.6
PAS·*pap*	$N3^+$−H2···$O1^-$	1.713	2.664	172.1
	N1−H5···O1	2.118	3.109	166.6
	N1−H6···O3	2.146	2.981	163.6
	N2−H3···O2	2.040	2.903	166.3
	C10−H11···O2	2.834	3.426	122.6
	N2−H4···π	2.521	3.295	153.9
PAS·*mhp*	$N2^+$−H1···$O1^-$	1.576	2.699	174.3
	O4−H2···O2	1.712	2.544	153.0
	N1−H3···O3	2.399	3.187	163.2
	N1−H4···O4	2.424	3.313	153.7
PAS·$(bpe)_{0.5}$	$N2^+$−H1···$O2^-$	1.779	2.650	175.2
	N1−H2···O2	2.444	3.188	144.4
	C13−H5···O1	2.430	3.093	128.2
	C11−H8B···π	3.413	3.934	115.8
PAS·*bpe*	O1−H1···N2	1.592	2.600	170.3
	N3−H3···N1	2.265	3.015	157.8
	C12−H10···O2	2.802	3.384	121.7
	C9−H9···O3	2.535	3.421	159.3
	N3−H4···π	2.952	3.739	148.8
PAS·*bpee*	O1−H1···N2	1.470	2.569	171.4
	N1−H3···N3	2.071	2.955	173.3
	C8−H8···O2	2.910	3.491	121.8
	C9−H9···O2	2.729	3.488	139.4
	N1−H4···π	2.564	3.375	149.3

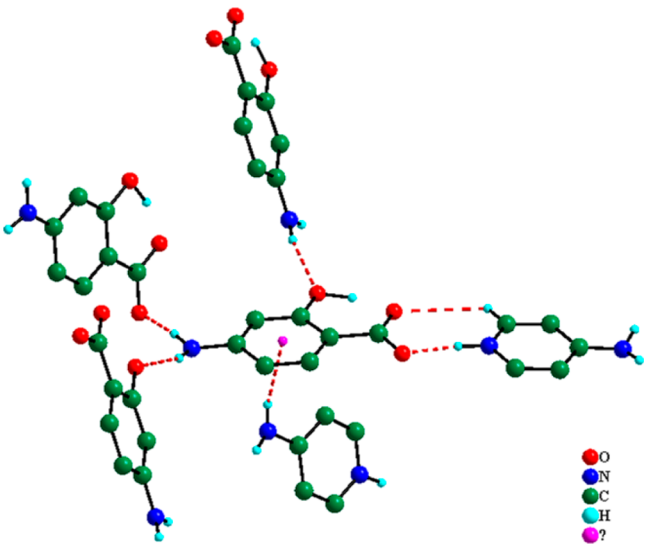

Figure 3. The hydrogen bond environment around PAS in 1:1 salt of PAS and *pap* (**3**). PAS^- and $papH^+$ are connected by synthon IV and N−H···π interactions. Notice that all the potential hydrogen bond functionalities of PAS are involved in hydrogen bonding interactions.

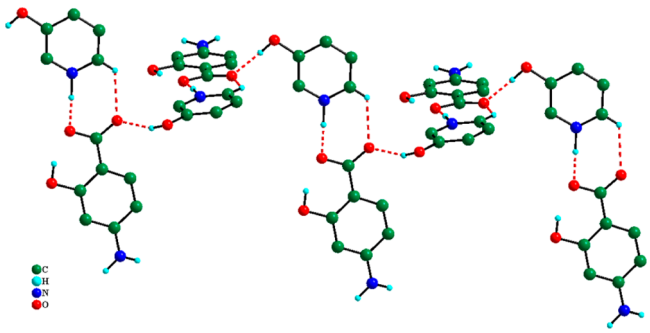

Figure 4. 1:1 Salt of PAS and *mhp* (**4**). The PAS^-−$mhpH^+$ dimer in **4** is similar to the one observed in **3**; the O−H···O interactions orient the dimers almost perpendicularly forming linear chains.

the structure. The trimer observed in this case is very similar to the one observed in **2** and **5**. The trimers in **6a** are linked to each other in a linear fashion via a bridging *bpe* molecule through N−H···N hydrogen bonds, whereas in **6**, the linear chains are formed by the assembly of dimers that are directly connected to each other by N−H···N interactions. Thus, in **6**, all the PAS molecules are oriented in one direction along the chain, while they are oppositely oriented in the chains of **6a**. This is the key difference between the two co-crystal polymorphs, **6** and **6a**. Co-crystal **7** was isolated when we opted for *bpee*, a rigid analogue of *bpe*. The structure of 1:1 co-crystal of PAS and *bpee*, **7**, is isostructural to **6a** (Figure 7 and Figure S10). A closer comparison of **6a** and **7** reveals that there are two types of *bpe* molecules in **6a** — the planar *bpe* connecting the PAS molecules in the trimer and the bent type connecting the trimers with the C═C−C−C torsion angles of 1.01 and −1.01° and 69.47 and −69.47° respectively, while in **7**, conformationally restricted planar *bpee* molecules are present in both the intra- and inter-trimer contacts. The flexibility around the C_{sp3}−C_{sp3} bond in *bpe* is probably responsible for the existence of co-crystal polymorphs of **6** and **6a**. In **6**, there is only one type of conformer and its geometry is even more bent (C═C−C−C) (torsion angles: 135.67 and 91.69°). However, unlike other crystals reported in this study, **7** invariably appeared with an impurity phase, which does not rule out the possibility of existence of other phase(s) that are yet to be identified.

Effect of Solvent in the Crystallization of PAS-Based Co-Crystals. When we changed the solvent from acetone to acetone−water mixture, we obtained concomitant crystals of **2** and **2a** in the case of *bpy*. Crystal structure analysis of **2a** revealed that it is similar to the compound reported earlier.[5a] The previous work reported the crystallization of **2a** from aqueous medium. Fourier map suggested that one of the pyridine molecules is protonated. In the crystal structure of **2a** (Figure S9), PAS^-−$bpyH^+$ dimers, connected by synthon V, aggregate to form infinite chains connected by N−H···N/O hydrogen bonds. These chains are interestingly interlinked via water molecules, generating an open square framework that is filled with the neutral *bpy* molecules. This clearly shows that for linear growth/aggregation of PAS and *bpy* molecules, either additional bridging pair of *bpy* molecules are required as in case of **2** or switching the orientation of one of the PAS molecules in the trimer is required with additional *bpy* and water molecules for close packing as in **2a**; otherwise, the discrete trimers end up close packing as in **1**. The results strongly suggest that the inclusion of solvent molecules at a supramolecular level is a

dx.doi.org/10.1021/cg3015332 | *Cryst. Growth Des.* XXXX, XXX, XXX−XXX

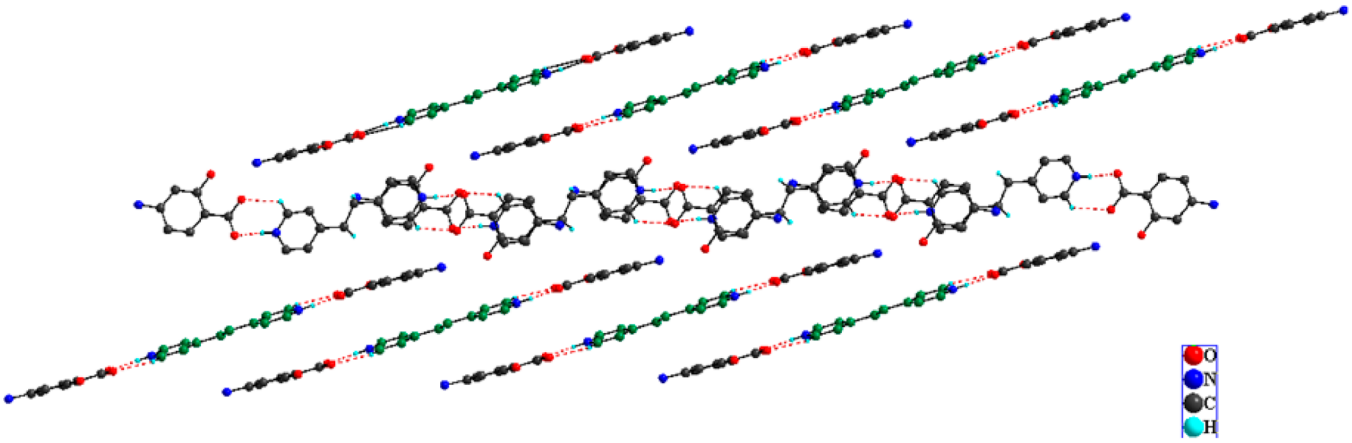

Figure 5. 2:1 salt of PAS and *bpe* (**5**). Discrete $PAS^{-}\cdots bpeH^{+}\cdots PAS^{-}$ trimers, formed through $COOH\cdots N_{heterocycle}$ synthon IV, are stacked in an inclined manner. Notice the occurrence of alternating stacks of the trimers, related by about 90° rotation about a horizontal axis generating a bilayer.

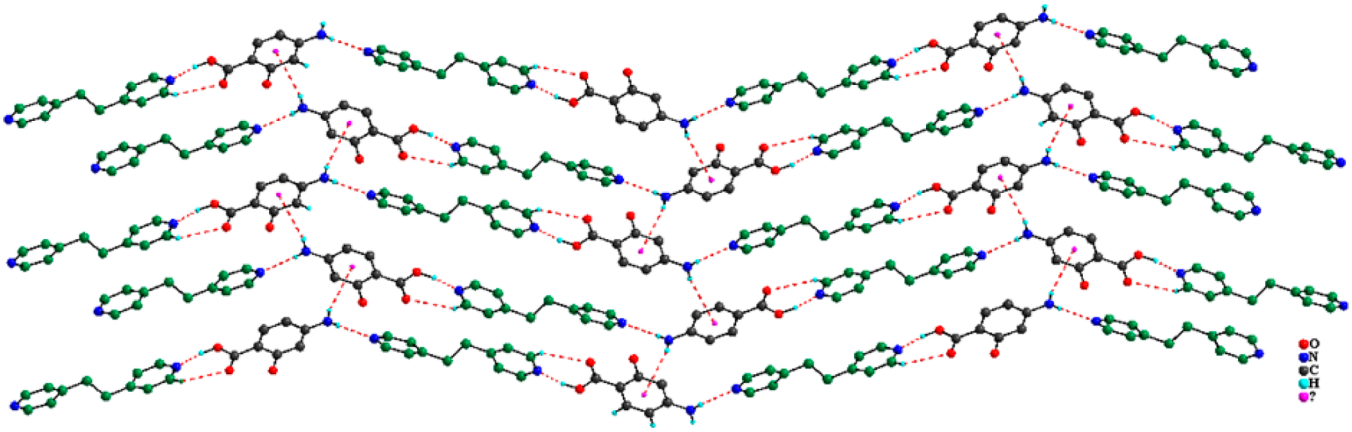

Figure 6. 1:1 Co-crystal of PAS and *bpe* (**6**). Interestingly, instead of PAS···*bpe*···PAS trimers as observed in **5**, PAS-*bpe* dimers are seen in **6**. Note that *bpe* is more flexible than *bpy*. The PAS-*bpe* dimers are connected by synthon II. These dimers are directly linked via N−H···N hydrogen bonds generating chains of alternating PAS and *bpe* molecules. In **6**, all the PAS molecules are oriented in one direction in the chains, while they are oppositely oriented in the chains of **6a**, a polymorph of **6**. Compare this with Figure S10. Notice the N−H···π interactions interlinking the chains.

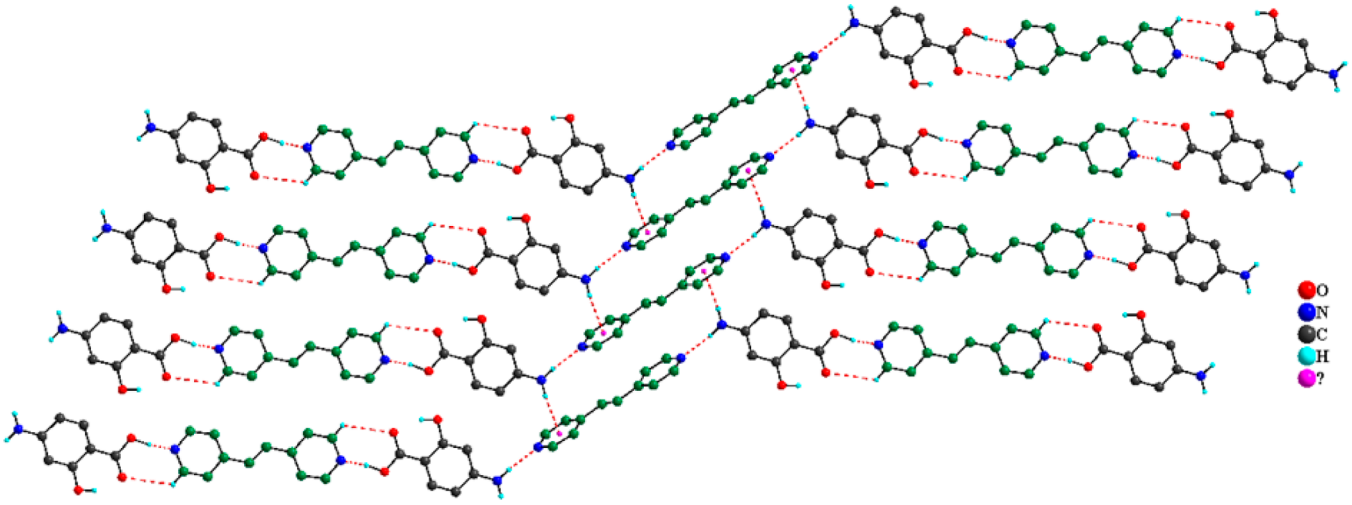

Figure 7. 1:1 Co-crystal of PAS and *bpee* (**7**). Note that *bpee* is conformationally more rigid than *bpe*. **7** is isostructural to **6a**. Compare this with Figure S10. The PAS···*bpy*···PAS trimers, connected by synthon II, generate chains of alternating PAS and *bpee* molecules connected by bridging *bpee* through N−H···N hydrogen bonds and the chains are interlinked via N−H···π hydrogen bonds.

careful engineering ploy that the system does to optimize various interactions.[15] Solvent had no effect in the case of *bpe* based co-crystals and the other solid forms reported herein. All nine of the solid forms were obtained by evaporating acetone solutions slowly at ambient conditions. The same results were obtained by slow evaporation of MeOH and acetone-MeOH

dx.doi.org/10.1021/cg3015332 | *Cryst. Growth Des.* XXXX, XXX, XXX−XXX

solutions. As discussed earlier in the previous sections, only the compositional variation led to the isolation of the three multicomponent crystals, of which two are co-crystal polymorphs and the third one is a salt with distinct stoichiomerty of PAS and *bpe* (Scheme 1 and Table 3); incidentally the reported polymorph **6a** was isolated from aqueous ethanolic medium.[5b]

The melting points of the PAS solid forms were found to range between 120 and 170 °C and lie above the corresponding starting materials (Table 3 and Figure S2). The Rietveld analysis of powder XRD of solids, **1** through **6**, confirm the monophasic nature of the bulk samples (Figure S3 through S8). The stretching mode of carbonyl group of free carboxylic acid is intense in co-crystals **1**, **2**, **6** and **7**, confirming the presence of neutral species in these solid forms, and found to be weak in salts **4** and **5**, while possibly merged with the aromatic C═N stretch in solid **3**. Thus, in salts, **3**−**5**, there is a possibility of occurrence of both neutral and ionic species.

CONCLUSION

We have shown that PAS-pyridine/*bpy* system exhibits rich structural diversity that includes salt, co-crystal, salt co-crystal/salt co-crystal hydrate and co-crystal polymorphs. Salt-co-crystal continuum cannot be ruled out in some of these cases. Solid solution formation between *bpe* and *bpee* is also currently being explored. The study demonstrates the robustness of $COOH\cdots N_{heterocycle}$ synthon and the utility of understanding structural landscape in terms of supramolecular synthon concept. There is a clear link between molecular and supramolecular aggregation, and this may correlate with the composition of the system. A trimer or a dimer connected by $COOH\cdots N_{heterocycle}$ synthon is primarily responsible for salt/co-crystal formation, while the stoichiometry of the resulting solids is governed by conformational flexibilty and/or supramolecular aggregation.

ASSOCIATED CONTENT

Supporting Information

Crystallographic information files (CIF) for **1**−**7**, ATR-FTIR spectra (Figure S1) for PAS, and **1**−**7**, DSC scans (Figure S2) for solids **1**−**6**, Rietveld refinement plots for **1**−**6** (Figures S3−S8), and crystal structures for solid **2a** (Figure S9) and **6a** (Figure S10). This information is available free of charge via the Internet at http://pubs.acs.org.

AUTHOR INFORMATION

Corresponding Author

*E-mail: aramanan@chemistry.iitd.ac.in (A.R.), ramthaimattam@yahoo.com (R.T.). Tel: +91-11-26591507. Fax: +91-11-26581102.

Notes

The authors declare no competing financial interest.

ACKNOWLEDGMENTS

P.K.G. thanks UGC for a research fellowship and A.R. acknowledges DST, Government of India, for financial support and the powder and single crystal X-ray diffraction facility at the Department of Chemistry, IIT Delhi, India.

REFERENCES

(1) (a) Shan, N.; Zaworotko, M. J. *Drug Discovery Today* **2008**, *13*, 440−446. (b) Blagden, N.; Matas, M. D.; Gavan, P. T.; York, P. *Adv. Drug Delivery Rev.* **2007**, *59*, 617−630. (c) Schultheiss, N.; Newman, A. *Cryst. Growth Des.* **2009**, *9*, 2950−2967. (d) Chen, J.; Sarma, B.; Evans, M. B. J.; Myerson, A. S. *Cryst. Growth Des.* **2011**, *11*, 887−897. (e) Eddleston, M. D.; Jones, W. *Cryst. Growth Des.* **2010**, *10*, 365−370. (f) David, S. E.; Timmins, P.; Conway, B. R. *Drug Dev. Ind. Pharm.* **2012**, *38*, 93−103.

(2) (a) Verreck, G.; Decorte, C.; Heymans, K.; Adriaensen, J.; Liu, D.; Tomasko., D.; Arien, A.; Peeterse, J.; Mooter, V. M. G.; Brewster, M. E. *Int. J. Pharm.* **2006**, *327*, 45−50. (b) Andre, V.; Braga, D.; Grepioni, F.; Duarte, M. *Cryst. Growth Des.* **2012**, *12*, 3082−3090.

(3) (a) Aakeroy, C. B.; Fasulo, M. E.; Desper, D. *Mol. Pharmaceutics* **2007**, *4*, 317−322. (b) Morissette, S. L.; Almarsson, O.; Peterson, M. L.; Remenar, J. F.; Read, M. J.; Lemmo, A. V.; Ellis, S.; Cima, M. J.; Gardner, C. R. *Adv. Drug Delivery Rev.* **2004**, *56*, 275−300. (c) Reddy, L. S.; Bethune, S. J.; Kampf, J. W.; Rodriguez, H. N. *Cryst. Growth Des.* **2009**, *9*, 378−385. (d) He, G.; Chow, P. S.; Tan, R. B. H. *Cryst. Growth Des.* **2009**, *9*, 4529−4532.

(4) (a) Garcia, H. C.; Diniz, R.; Oliveira, L. F. *CrystEngComm* **2012**, *14*, 1812−1818. (b) Braga, D.; Grepioni, F.; Andre, V.; Duarte, M. T. *CrystEngComm* **2009**, *11*, 2618−2621.

(5) (a) Garcia, H. C.; Cunha, R. T.; Diniz, R.; Oliveira, L. F. *J. Mol. Struct.* **2011**, *991*, 136−142. (b) Garcia, H. C.; Cunha, R. T.; Diniz, R.; Oliveira, L. F. *J. Mol. Struct.* **2012**, *1010*, 104−110.

(6) (a) Grobelny, P.; Mukherjee, A.; Desiraju, G. R. *CrystEngComm* **2011**, *13*, 4358−4364. (b) Desiraju, G. R. *Angew. Chem., Int. Ed.* **1995**, *34*, 2311−2327.

(7) Walsh, R. D. B.; Bradner, M. W.; Fleischman, S.; Morales, L. A.; Moulton, B.; Rodriguez, H. N.; Zaworotko, M. J. *Chem. Commun.* **2003**, 186−187.

(8) Bruker Analytical X-ray Systems, *SMART: Bruker Molecular Analysis Research Tool*, Version 5.618; Bruker AXS: Madison, WI, 2000.

(9) Bruker Analytical X-ray Systems, *SAINT-NT*, Version 6.04, Bruker AXS: Madison, WI, 2001.

(10) Bruker Analytical X-ray Systems, *SHELXTL-NT*, Version 6.10; Bruker AXS: Madison, WI, 2000.

(11) *DIAMOND*, Version 1.2c; Klaus, B., University of Bonn, Germany, 1999.

(12) *TOPAS V4.2: General Profile and Structure Analysis Software for Powder Diffraction Data*; Bruker AXS GmbH: Karlsruhe, Germany, 2009.

(13) (a) Lynch, D. E.; Chatwin, S.; Parsons, S. *Cryst. Eng.* **1999**, *2*, 137−144. (b) Du, M.; Zhang, Z. H.; Guo, W.; Fu, X. J. *Cryst. Growth Des.* **2009**, *9*, 1655−1657. (c) Shattock, T. R.; Arora, K. K.; Vishweshwar, P.; Zaworotko, M. J. *Cryst. Growth Des.* **2008**, *8*, 4533−4545. (d) Men, Y. B.; Sun, J.; Huang, Z. T.; Zheng, Q. Y. *CrystEngComm* **2009**, *11*, 978−979.

(14) (a) Nichol, G. S.; Clegg, W. *Cryst. Growth Des.* **2009**, *9*, 1844−1850. (b) Pedireddi, V. R.; Ranganathan, A.; Chatterjee, S. *Tetrahedron Lett.* **1998**, *39*, 9831−9834. (c) Bowers, J. R.; Hopkins, G. W.; Yap, G. P. A.; Wheeler, K. A. *Cryst. Growth Des.* **2005**, *5*, 727−736. (d) Dickie, D. A.; Schatte, G.; Jennings, M. C.; Jenkins, H. A.; Khoo, S. Y. L.; Clyburne, J. A. C. *Inorg. Chem.* **2006**, *45*, 1646−1655.

(15) Upreti, S.; Datta, A.; Ramanan, A. *Cryst. Growth Des.* **2007**, *7*, 966−971.